

Optimal Output Level Selection for Multilevel Halftoning Based on Visual Experiments Using Spatially Modulated Gratings

Muge Wang[▲]

Foxlink Peripherals Inc., Fremont, California USA

Kevin J. Parker

University of Rochester, Dept. of Electrical and Computer Engineering, Rochester, New York, USA

Kevin Spaulding

Eastman Kodak Company, Imaging Science Division, Rochester, New York, USA

Qing Yu

Vimicro Corporation, Mountain View, California, USA

Rodney Miller

Eastman Kodak Company, Imaging Science Division, Rochester, New York, USA

Experiments have shown that multitone with output levels equally spaced in CIE L^* does not produce uniform texture at different gray levels. In this study, psychophysical experiments are described, investigating the influence of spatial modulation on the perception of lightness difference. A variety of different patterns (square wave, checker-board, and 50% blue noise patterns) were tested at various frequencies and amplitudes (contrast). A significant frequency dependent effect was observed where the lightness difference perception is reduced for high frequency modulated gratings at low L^* values. The magnitude of this effect is highly related to the frequency of the modulation. There is no evidence to indicate that either modulation type or modulation amplitude has a significant effect on the lightness difference perception. Based on the experimental results, an effective lightness metric (L_e^*) is derived as a function of spatial frequency. The L_e^* metric is intended to provide a space that is linearly related to lightness difference perception for frequency modulated patterns. Results from a further visual experiment have verified that multitone patterns produced using levels that are equally spaced in L_e^* produces results with more uniform texture visibility across the entire tone scale.

Journal of Imaging Science and Technology 47: 309-326 (2003)

Introduction to Multilevel Halftoning

Multilevel halftoning is an extension of bi-level halftoning, which uses black, white, and one or more middle gray levels to produce the appearance of continuous tone images. Algorithms for halftoning and multitone are very similar. Most bi-level halftoning techniques can be readily generalized and extended to multilevel halftoning by replacing the threshold operation in bi-level halftoning with a quantization operation.^{1,2} The diagram for multitone using a stochastic screen is illustrated in Fig. 1.

If the input image $i(x,y)$ has p possible input levels, the output image has q possible output levels, and the dither matrix $d(x,y)$ has m levels, then the output image $o(x,y)$ can be given by:

$$o(x,y) = INT \left[\frac{q-1}{p-1} i(x,y) - \frac{d(x_d, y_d)}{m-1} + 1 \right], \quad (1)$$

where INT is the integer truncation operator, and (x_d, y_d) is the dither matrix address computed by applying a modulo operation to the pixel address (x, y) . It can be easily shown that the above equation is equivalent to the conventional halftone threshold operation when the output level $q = 2$ and $p = m$.

The selection of the intermediate output levels will have a direct effect on the visibility of the resulting multitone patterns. The most obvious way to select the intermediate levels is to let the output levels be equally spaced in CIE L^* , because the L^* function defined in CIELAB color

Original manuscript received July 18, 2002

▲ IS&T Member

©2003, IS&T—The Society for Imaging Science and Technology

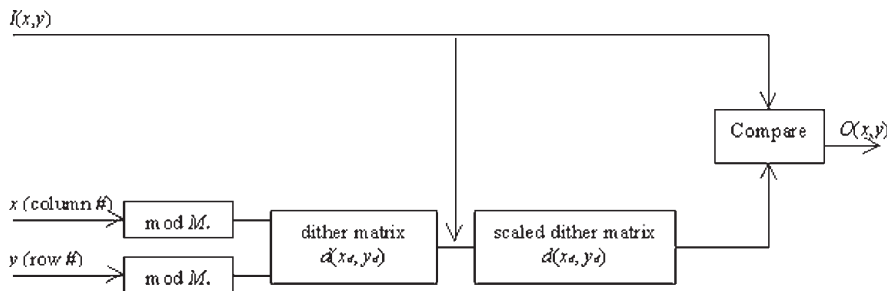


Figure 1. Multilevel halftoning using a stochastic screen.

space was designed to be linearly related to the human visual perception of luminance.³ A patch with an L^* value twice that of a reference patch would be perceived to be twice as bright as the reference patch. Similarly, equal differences in L^* values would result in equal differences in brightness perception. Thus, if the output levels are chosen to be equally spaced in L^* space, we would expect to obtain results where the perceived brightness modulation, and therefore the visibility of the multitone patterns, would be independent of lightness level. However, experimental results have shown that the visibility of the resulting multitone patterns for a gray ramp produced by this method is not uniform. In particular, the multitone patterns are more visible at high L^* values than at low L^* values.⁴ This leads to the hypothesis that while the L^* function was developed based on the estimation of perceived lightness of large area uniform patches, it may not be suitable to characterize the perception of lightness differences for applications where the stimuli are presented at high spatial frequencies. Thus, the understanding of the perception of lightness difference at high-spatial frequencies is essential for high-quality multitone reproduction. Little research has been reported to study supra-threshold human perception of lightness differences under high spatial frequencies.

Based on the above considerations, we designed a psychophysical experiment to investigate supra-threshold lightness difference perception for modulated signals as a function of spatial frequency and amplitude.⁵ Our particular interest is to define an effective lightness space that can be applied to the selection of the output levels for multitone. The effective lightness space (L_e^*) will have the property that it is linearly related to the lightness difference perception for spatially modulated patterns. Therefore, multitone patterns that are produced using intermediate output levels that are equally spaced in effective lightness are expected to have uniform texture visibility across the tone scale.

A Study of Lightness Difference Matching with Square-wave Gratings

In this section, a psychological experiment is described that was used to study the visual perception for square wave gratings modulated at various frequencies and amplitudes. The effect of modulation frequency and amplitude will provide us a better understanding of the visual perception as a function of printing resolution and the number of the multitone output levels. Experiments using more complicated spatially modulated gratings will be discussed in the next section.

Experimental Design

Apparatus

The stimuli were presented on a 20 in. non-interlaced Barco monitor. The resolution of the monitor was 1152 by 900 at 80 dpi (dot per inch). The monitor was characterized using a Photo Research PR-705 SpectraScan tele-spectroradiometer at 14.2 ft. from the monitor, which was the viewing distance of the experiment. The measured luminance was converted to L^* value, and a look-up table from code value to L^* value was generated.

The formula used to convert luminance to lightness is:^{3,6}

$$L^* = \begin{cases} 116 \left(\frac{Y}{Y_n} \right)^{1/3} - 16 & \text{if } \left(\frac{Y}{Y_n} \right) > 0.008856 \\ 903.3 \left(\frac{Y}{Y_n} \right) & \text{otherwise} \end{cases}, \quad (2)$$

where Y is luminance and Y_n is the luminance of the white point of the monitor.

Subjects

Five observers participated in this experiment. MW, the principal author, repeated the experiment twice. Two other co-authors, QY and RM, took part in the experiment. The other two observers were HL (an experienced observer), and SD (an inexperienced observer). Neither HL nor SD had prior knowledge of the design of the experiment.

Stimuli

The experiment was based on a lightness difference matching paradigm. The stimuli used in the experiment were horizontal square wave gratings with various spatial frequencies and modulated lightness amplitudes. The task of the observer was to compare the perceived lightness modulation of a standard patch to that of a test patch, and to adjust the modulation amplitude of the test patch until the perceived lightness modulation was equal to that of the standard patch. The modulation amplitude is defined as $\Delta L^* = L_1^* - L_2^*$, where L_1^* and L_2^* are the lightness values of the bright bars and dark bars, respectively. The standard patch and the test patch each subtended a visual angle of 2° at the observing distance of 14.2 ft. The stimuli were displayed in a complex field that consisted of randomly placed squares with random sizes and gray levels. We designed this complex pattern to reduce the effect of global adaption and patch edge effects on the lightness modulation

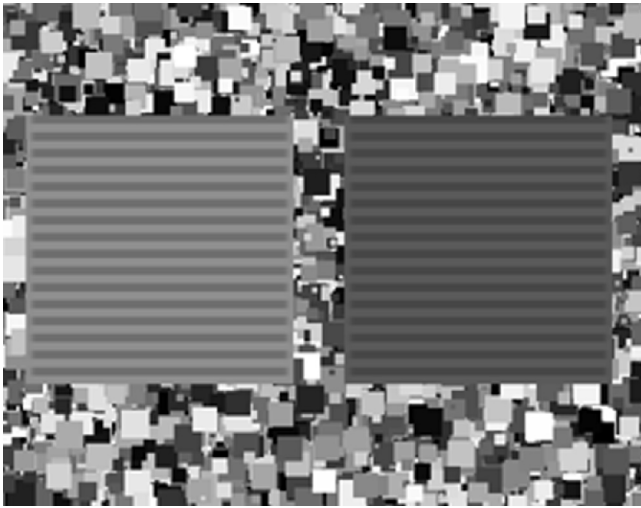


Figure 2. The complex background and the stimuli. The grating on the left is the standard patch and the grating on the right is the test patch.

preception. The mean luminance of this random background pattern was 21.1 cd/m^2 . The square wave pattern was blurred near the boundaries of the patches. A typical grating pair along with the complex background is illustrated in Fig. 2.

One concern with this stimulus configuration is whether the complex background will cause a resulting contrast reduction. Simple calculations show that the visual angle of the entire monitor was $4.8^\circ \times 3.8^\circ$, whereas each stimulus (the test stimulus and the standard stimulus) subtended an angle of $2^\circ \times 2^\circ$. Thus, the stimuli occupied a large portion of the screen. The large area of stimulus compared to the area of the entire background minimizes the contrast reduction caused by the background.⁷ Furthermore, the background and the stimuli have different frequency characteristics. According to Ejima and Takahashi's analysis that the spatial frequency selective mechanism plays an important role in contrast reduction,⁸ the broad frequency spectrum of the complex background should not cause a significant inhibitory interaction for a particular frequency. Therefore, the effect of the complex background should be small on the perceived contrast of the stimuli.

Experimental Procedure

The observers viewed the monitor binocularly in a dark room. The experiment began after several minutes of adaptation of the dark surroundings and a short practice session. The entire experiment was divided into three sessions. The observer was allowed to take a short break between the sessions if necessary. The average time to complete the entire experiment was ninety minutes.

In each session, the perceived lightness modulation for a predetermined amplitude was examined at three different spatial frequencies. The average lightness value of the standard patch was set at $L^* \approx 50$, and ΔL^* , the amplitude of the lightness modulation for the standard patch, was set to 6.39, 12.7, and 25.5 L^* units for the three sessions, respectively. These differences corresponded to about 1/16, 1/8, and 1/4 fractions of the entire L^* range, and these settings are perceptually similar to multitone images produced using 16, 8, and 4 output levels, respectively. The frequencies for the three

Table I. The Settings (Frequency and Contrast) of the Experiment.

	Sub-session 1	Sub-session 2	Sub-session 3
Session 1: $\Delta L^* = 6.39$	8 cpd	12 cpd	0.5 cpd
Session 2: $\Delta L^* = 12.7$	8 cpd	15 cpd	0.5 cpd
Session 3: $\Delta L^* = 25.5$	12 cpd	20 cpd	0.5 cpd

modulation amplitude settings are listed in Table I. The patterns of the very low frequency (0.5 cycle per degree (cpd)) were bipartite patches that were used to verify the lightness difference perception of solid patches. The adjustment in the spatial frequencies for different amplitudes was introduced to ensure that the patterns remained supra-threshold while exploring the largest possible frequency range.

Each session was comprised of three sub-sessions, where in each sub-session the experimental patches with the frequencies listed in Table I were displayed in the order from sub-session 1 to sub-session 3. Within each of the nine sub-sessions, a fixed standard patch was used. The frequency and the modulation amplitude of the standard patch were consistent with the frequency and modulation amplitude settings of the sub-session, and its average lightness was fixed at $L^* \approx 50$. The test patches had the same frequency and modulation amplitude as the settings of the sub-session as well, however, their average lightness values were varied across the entire lightness scale. For each sub-session, there were 11 test patches and their initial average lightness values were designed to cover the entire lightness scale as much as possible. The initial lightness modulation of the test patches was chosen to be equal to the ΔL^* of the standard patch plus a randomized difference, which could be either positive or negative. Test patches were first presented in an ascending lightness order, and then in a descending lightness order. The observer was asked to adjust the amplitude of the lightness modulation of the test patch until its perceived lightness difference matched the perceived lightness difference of the standard patch. The observer used the keyboard to make the adjustment where the up and down arrow keys were used for large adjustments ($\pm 5 L^*$ units), and the left and right arrow keys were used for small adjustments ($\pm 1 L^*$ unit). Each test patch was presented twice in the sub-session. Before the sub-session ended, the differences between the matched amplitudes of the same test patch were calculated, and the three patches that resulted in the highest variations in the two rounds were tested one more time to reduce the uncertainty of the data.

Results

In total, there were six observations from five subjects. The mean results and the standard errors from all the six observations are plotted in Fig. 3. The x -axis in the figure is the average lightness L^* of the test patches, and the y -axis is the lightness difference of the test patches that have the same perceived lightness difference as that of the standard patch. In the figure, there are three groups of curves of which each of them is comprised of three curves. From the top to the bottom, the three groups of curves represent the results from the largest ΔL^* to the smallest ΔL^* , respectively. The results for the low frequency (0.5 cpd) of all the three sessions are plotted as solid lines, those of the middle frequencies are plotted as long dashed lines, and those of the

TABLE II. The p-Values of the Two-Tailed Student T-Test.

session 1: $\Delta L^* = 6.39$		sequence numbers									
p-value	1	2	3	4	5	6	7	8	9	10	11
f = 0.5, 8 cpd	0.256	0.239	0.272	0.522	0.824	0.664	0.802	0.145	0.296	0.491	0.568
f = 8, 12 cpd	0.023	0.011	0.019	0.599	0.172	0.344	0.361	0.062	0.809	0.244	0.900
session 2: $\Delta L^* = 12.7$		sequence numbers									
p-value	1	2	3	4	5	6	7	8	9	10	11
f = 0.5 and 8 cpd	0.264	0.081	0.527	0.762	0.762	0.687	0.015	0.077	0.828	0.236	0.905
f = 8 and 15 cpd	<0.001	0.004	0.001	0.604	0.017	0.386	0.178	0.503	0.148	0.512	0.313
session 3: $\Delta L^* = 25.5$		sequence numbers									
p-value	1	2	3	4	5	6	7	8	9	10	11
f = 0.5 and 8 cpd	0.002	0.003	0.046	0.406	0.720	0.194	0.877	0.389	0.933	0.546	0.507
f = 8 and 12 cpd	0.022	<0.001	0.041	0.072	0.462	0.595	0.766	0.595	0.324	0.103	0.784

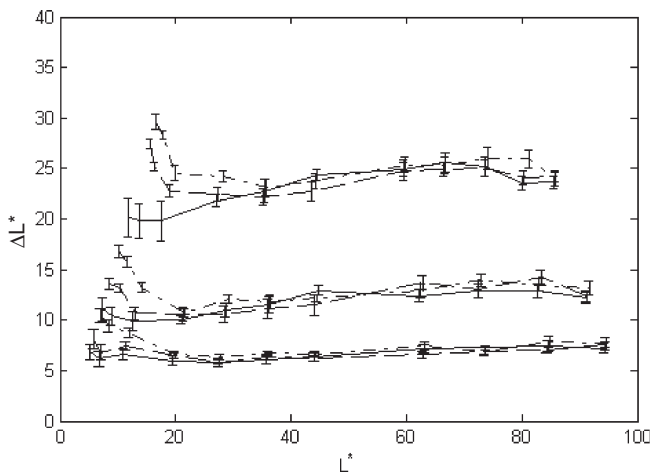


Figure 3. The average results and the standard errors of the six observations for square wave gratings. For the groups of curves from the bottom to the top, the amplitudes were: $\Delta L^* = 6.39$, $\Delta L^* = 12.7$, and $\Delta L^* = 25.5$, respectively. For the group of curves on the bottom: solid line: 0.5 cpd, dashed line: 8 cpd, and dotted line: 12 cpd; for the group of curves on the center: solid line: 0.5 cpd, dashed line: 8 cpd, and dotted line: 15 cpd; for the group of curves on the top: solid line: 0.5 cpd, dashed line: 12 cpd, and dotted line: 20 cpd.

high frequencies are plotted as short dashed lines. Thus, each single curve represents the matched lightness difference as a function of the average lightness for a particular modulation amplitude and frequency.

A data point at a particular position (L^* , ΔL^*) indicates that a pattern with an average lightness of L^* and a lightness difference of ΔL^* produced the same perceived lightness modulation as the standard patch of the same spatial frequency. We will refer to the lightness difference of the standard patch as the “effective lightness difference” ΔL_e^* because the lightness differences of the test patches were effectively perceived to be equal. All the points on one curve had the same ΔL_e^* . Thus each curve reflects the relationship between the perceived lightness difference and L^* values at a given frequency and amplitude. If there were no frequency-dependent lightness difference perception effects, we would expect these curves to be horizontal lines, and that the curves for the various frequencies would lie on top of each other.

Analysis Observations

Several observations can be made upon examination of Fig. 3. First, all the high frequency curves (the frequencies other than 0.5 cpd, with long dashed lines indicating lower frequencies and short dashed lines indicating higher frequencies) bend upward for low L^* values ($\sim L^* < 30$). There is a trend from low frequencies to high frequencies in the low L^* region. The curves for different frequencies separate and arrange themselves in the order of the frequency values. The higher the frequency, the further its data are apart from the flat line, indicating the frequency effect on lightness difference perception increases with spatial frequency. Second, there was no obvious trend at higher L^* values, where all the curves tend to be relatively flat.

A two-tailed student *t*-test was used to compare the results from all the observations between 0.5 cpd and the middle frequency, and between the middle frequency and the high frequency for each session. The *p*-values (level of significance) of the test are listed in Table II. The null hypothesis H_0 is that the mean of the two distributions are equal and the alternative hypothesis H_1 is that the mean of the two distributions are not equal. The sequence numbers from 1 to 11 in Table II correspond to the sequence numbers of the test patches with smaller number indicating lower average lightness values and larger numbers indicating higher average lightness values. Because the average lightness values of the matched patches will change along with the matched amplitudes, it impossible to compare the results as the function of the average lightness value. However, the test between the same sequence numbers can still provide us meaningful results. Note that for sequence numbers smaller than 3, most of the *p*-values are very small (< 0.05), whereas for sequence numbers larger than 3, most of the *p*-values are fairly large. Therefore, the statistical test results suggest the frequency dependent matched lightness differences are significantly different at low L^* , but not at middle and large L^* . By inspecting Fig. 3, it can be roughly estimated that the frequency effect can be observed up to $L^* = 30$.

The upward bending of the high-frequency curves at low L^* values means that, in order to produce the same effective lightness difference as that of the patch with high average L^* value, a larger ΔL^* must be used for the patches with low average L^* value. In other words, the effective lightness difference is reduced at low L^* values for high frequency stimuli. The data have also shown that the magnitude of the effect is larger for higher fre-

quencies. The effect of reduced effective lightness difference at low L^* is consistent with the observation made in the multitone experiment that equal ΔL^* multitone patterns are more visible at high L^* than at low L^* .⁴ A similar phenomenon was reported by Peli et al., where a low pass characteristic of apparent contrast was found at low luminance levels.⁹

It is also interesting to note that the very low frequency curves were not strictly horizontal lines, as would be expected according to the assumption that the L^* function can be used to predict lightness differences for large area patches. One possible reason for this could be that the viewing conditions (such as stimuli luminance level, background/surround luminance levels and the size of the stimuli) were not identical to those under which the lightness function was originally derived. In particular, the surround luminance is known to have a significant effect on perceived brightness, so the fact that the stimuli were viewed in a dark room could be a significant factor.

Effective Lightness Space L_e^*

Based on the experimental results, we can derive an effective lightness L_e^* as a function of the conventional lightness L^* and the spatial frequency. The first step is to determine the derivatives of the effective lightness L_e^* versus the conventional lightness L^* . The experimental data on the same curve correspond to equal effective lightness differences. Suppose for one curve, the average lightness and the modulation amplitude of the matched patches were $(L_1^*, \Delta L_1^*)$, $(L_2^*, \Delta L_2^*)$, ..., $(L_n^*, \Delta L_n^*)$, and their effective lightness differences were ΔL_{e1}^* , ΔL_{e2}^* , ..., ΔL_{en}^* , respectively. Since all the patches had the same perceived lightness differences as the standard patch, we have:

$$\Delta L_{e1}^* = \Delta L_{e2}^* = \dots = \Delta L_{en}^* = \Delta L_{e0}^*, \quad (3)$$

where the number 1 to n denote the sequence numbers of the measured data and ΔL_{e0}^* is the effective lightness difference of the standard patch. Furthermore, the differentiation of L_e^* with respect to L^* at L_i^* ($i = 1, 2, \dots, n$) can be approximated by:

$$\frac{dL_e^*}{dL^*} \approx \frac{\Delta L_{ei}^*}{\Delta L_i^*} = \frac{\Delta L_{e0}^*}{\Delta L_i^*}. \quad (4)$$

Because ΔL_{e0}^* is an undetermined constant in each particular session, the differential equation can be expressed by:

$$\frac{dL_e^*}{dL^*} = \text{cons.}^* \frac{1}{\Delta L_i^*} \quad (5)$$

Using the above equation, we can plot the first-order derivative of L_e^* with respect to L^* for the three amplitudes, $\Delta L_0^* = 6.39$, 12.7 and 25.5 , under varying frequencies. Figure 4 illustrates the approximated dL_e^*/dL^* based on the experimental data for $\Delta L_0^* = 6.39$, 12.7 , and 25.5 , respectively. For these plots, the constant in Eq. 5 was chosen to be the ΔL_0^* of the standard patch. The measured data were plotted as isolated points in the figures. Then we fitted the isolated points with smooth curves with least squares fitting. The functional form used for the curve fitting was:

$$f\left(\frac{dL_e^*}{dL^*}\right) = (a_1 + a_2 L^*) \left(1 - a_3 \exp(-a_4 L^{*2})\right), \quad (6)$$

where a_1 is a general factor, which controls the small drift of the function around 1, a_2 is used to take account of the slight drop of the derivatives at the high L^* end, a_3 describes the degree that the curve deviates from 1 at low L^* end, and a_4 influences the position of the transition from reduced lightness difference perception to normal lightness difference perception. The fitted curves are plotted in the same figure.

Finally, the relationship between the effective L_e^* and the conventional L^* was obtained by performing a numerical integration of the derivative functions plotted in Fig. 4. Boundary conditions were applied so that $L_e^* = 0$ when $L^* = 0$, and $L_e^* = 100$ when $L^* = 100$. The resulting L_e^* versus L^* curves are plotted in Fig. 5.

Besides the frequency effect, the influence of amplitude modulation for a constant frequency is also of interest. The average L_e^* ($f = 8$ cpd) at $\Delta L^* = 6.39$ and $\Delta L^* = 12.7$ and the average L_e^* ($f = 12$ cpd) at $\Delta L^* = 6.39$ and $\Delta L^* = 25.5$ are plotted in Fig. 6 as solid line and dashed line, respectively. The error bars are the deviation of each individual L_e^* from the average L_e^* curve at the given frequency. Even with the deviation bars, the L_e^* ($f = 8$ cpd) and L_e^* ($f = 12$ cpd) can still be distinguished from each other. This suggests that the magnitude of the effect of modulation amplitude on the perception of lightness differences at frequencies examined in this study may not be as significant as that of the frequency effect. Since the frequency effect dominates the amplitude effect, then we may use frequency as the control variable for L_e^* , regardless the amplitude of the modulation. The L_e^* versus L^* curves for various frequencies are illustrated in Fig. 7. Each curve is the average of the curves with the same frequency but different amplitudes.

The Experiment with New Gratings: Checkerboard Gratings and Blue Noise Gratings

The Checkerboard and Blue Noise Gratings

The stimuli used in the previous experiment were square wave gratings modulated at various frequencies and amplitudes.⁵ Square wave gratings are one of the most commonly used targets in psychological experiments. However, square wave gratings are modulated in only one spatial direction. Halftone/multitone patterns are more complex than square wave gratings in the frequency domain. To confirm that the results developed using square wave gratings are valid for other types of stimuli (and thus can be directly applied to multitoning), we repeated the experiment with two new types of stimuli that were modulated in two dimensions instead of one. These stimuli were checkerboard gratings and 50% blue noise patterns. The checkerboard gratings are equivalent to the 50% dot pattern that would be formed with a Bayer dither multitoning algorithm. Similarly, the blue noise patterns are analogous to the patterns that would be created using multitone algorithms based on error diffusion or stochastic dither techniques. The checkerboard and blue noise gratings used in the experiment are illustrated in Fig. 8.

The Apparent Frequency of the Stimuli

In general, the frequency of square wave grating is considered as the fundamental frequency in the Fourier analysis. Its fundamental frequency can be easily de-

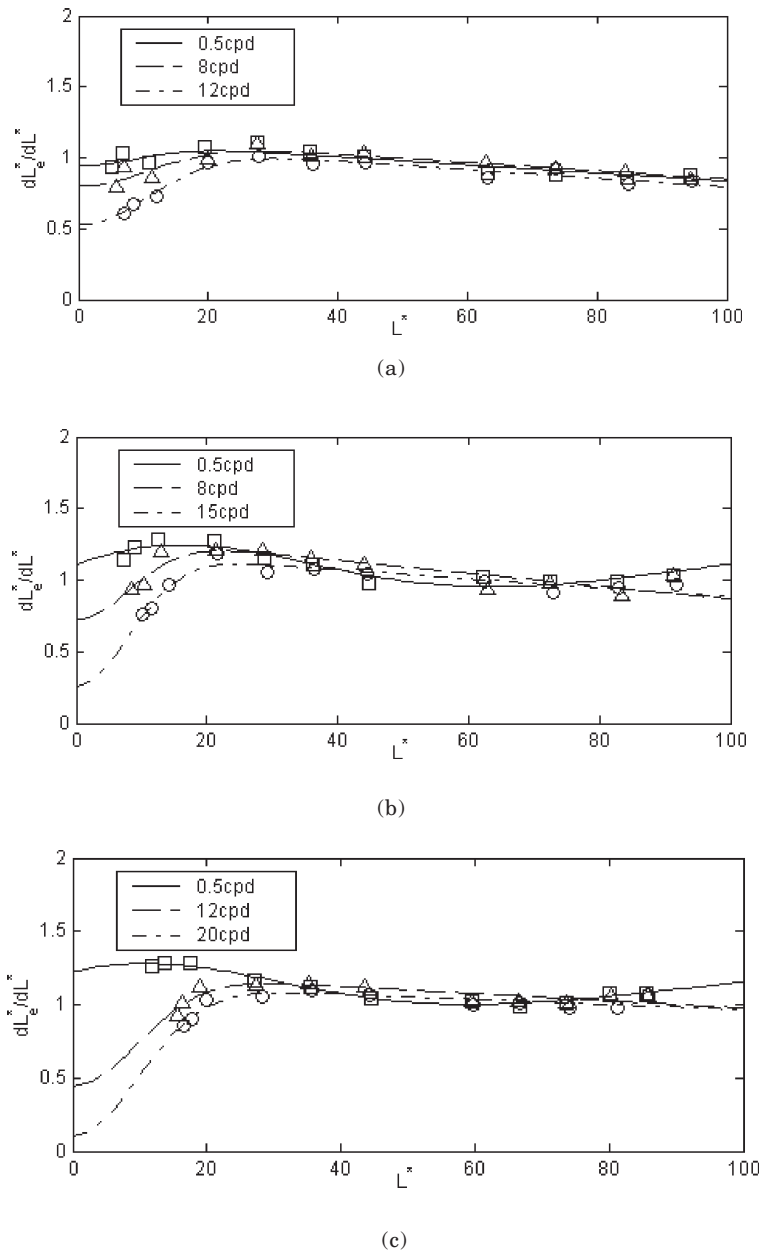


Figure 4. dL_e^*/dL^* . (a) $\Delta L_0^* = 6.39$, (b) $\Delta L_0^* = 12.7$, and (c) $\Delta L_0^* = 25.5$. Square wave grating.

rived from the geometrical relationship of the size of the grating and the viewing distance. The unit of cycle per degree (cpd), i.e., the number of cycles per unit visual angle,¹⁰ is often used to describe this frequency value. In our experiment, the viewing distance was set as 14.2 ft. (170.4 in.) and the size of the grating is 480 pixels by 480 pixels, the resolution of the monitor is 80 dpi. So the stimuli spanned an angular range of $2^\circ \times 2^\circ$. Thus the spatial frequency in cycles per degree would be given by the number of the cycles on the square wave gratings divided by 2. If the thickness of the horizontal bars of the square waves is w pixels, then the frequency in cpd of the square wave gratings can be calculated by:

$$f_{eff} = \frac{480/w}{\frac{480/80}{170.4} * \frac{180}{\pi}} \approx \frac{120}{w} \text{ cpd}$$

For checkerboard and blue noise patterns, it is necessary to define a single value “apparent frequency” for the checkerboard gratings and blue noise patterns, so that it is comparable with the frequency of the square wave gratings. We used dominant frequency of the radial average power spectrum (RAPS) to represent the “apparent frequency” of the grating.¹¹ Let f_i and f_j denote the spatial frequency in the horizontal and vertical directions, respectively. The radial frequency f_r is

$$f_r = \frac{\sqrt{(f_i)^2 + (f_j)^2}}{s(\theta)}, \quad (7)$$

whereas $\theta = \arctan(f_j/f_i)$ is the orientation of the frequency and $s(\theta) = 0.15\cos(4\theta) + 0.85$. Let $PS(i, j)$ denote the power spectrum of the frequency (i, j) , and $N_r(f_r)$

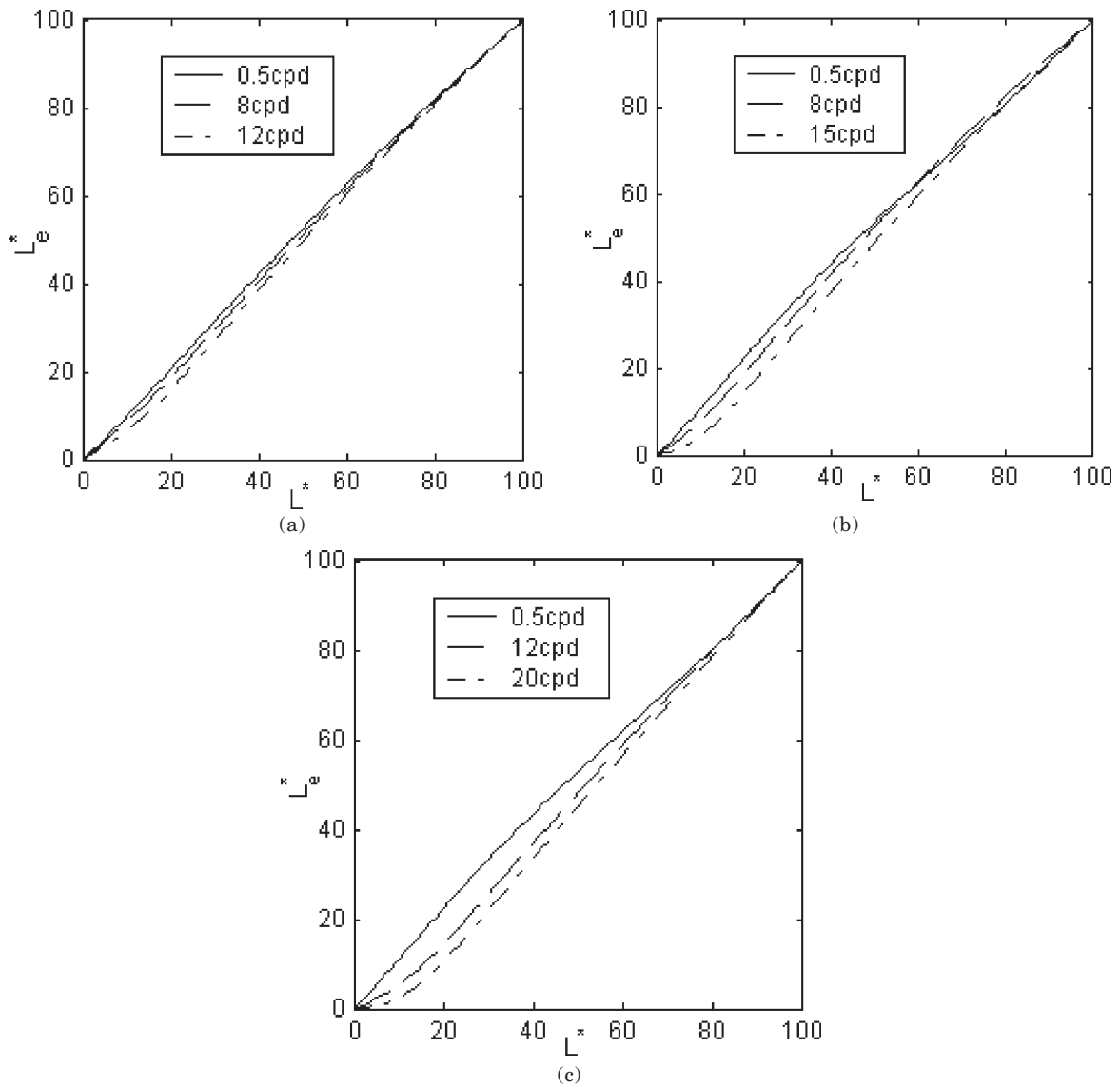


Figure 5. L_e^* versus L^* . (a) $\Delta L_0^* = 6.39$, (b) $\Delta L_0^* = 12.7$, and (c) $\Delta L_0^* = 25.5$. Square wave grating.

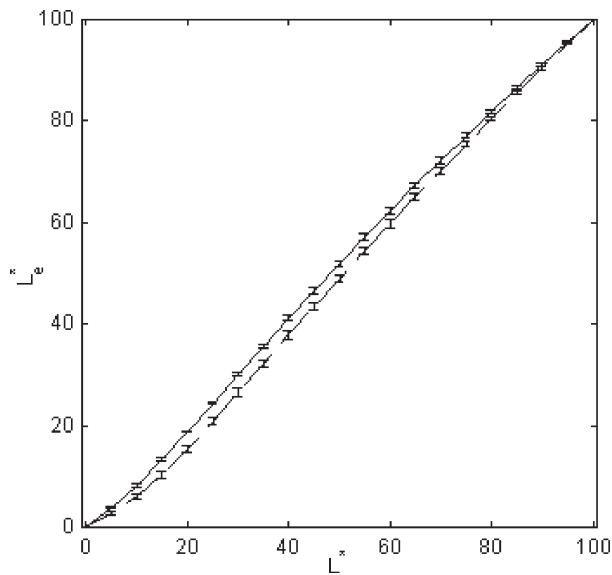


Figure 6. Average L_e^* (multiple amplitudes) and the deviation from the average L_e^* vs L^* under frequencies 8 cpd (solid line) and 12 cpd (dashed line).

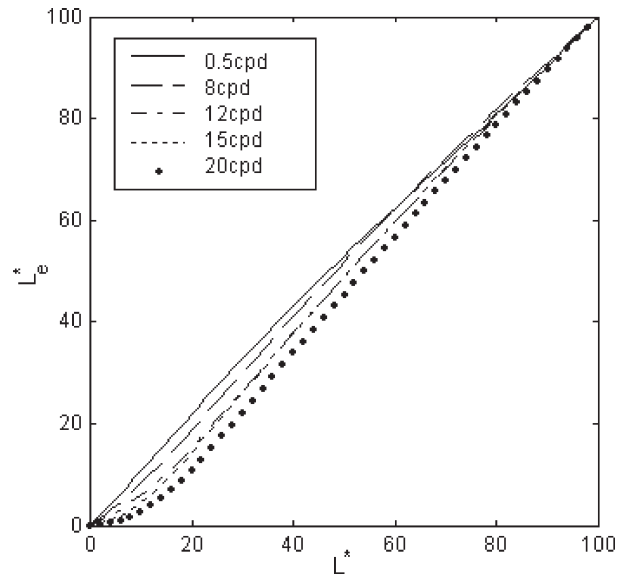


Figure 7. The average results as the function of frequency only. Square wave grating.

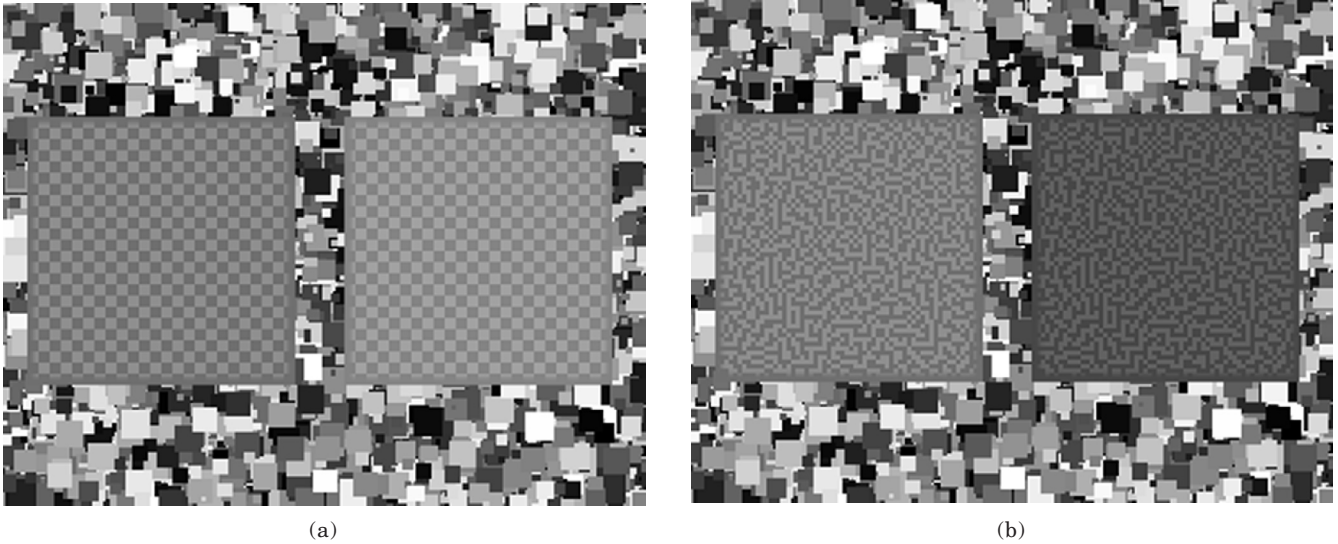


Figure 8. The illustration of the new stimuli. (a): checkerboard gratings, and (b): 50% blue noise gratings. The grating on the left is the standard patch and the grating on the right is the test patch.

denote the number of the discrete frequency samples in an annulus. Then the RAPS is:

$$RAPS(f_r) = \frac{1}{N_r(f_r)} \sum_{INT(\sqrt{f_i^2 + f_j^2}) = f_r} PS(i, j) \quad (8)$$

It was found that the three types of stimuli did not have the same apparent frequency when they were modulated by the same unit feature size. (For square wave gratings, the unit feature size is the same as the thickness of the horizontal bars, and for checkerboard and blue noise gratings, the unit feature size is the same as the size of the single dot, in terms of the number of pixels.) The analysis of the RAPS shows that the square wave gratings, checkerboard gratings and 50% gray blue noise patterns have approximately the same apparent frequencies (peak frequencies) when the ratio of their unit feature sizes was 1:2:0.8. For example, the checkerboard patterns and blue noise patterns in Fig. 8 exhibit about the same apparent frequencies. The RAPS of the square wave, checkerboard gratings and blue noise patterns that have the same apparent frequencies are illustrated in Fig. 9. In Fig. 9, the three types gratings have the same dominant radial frequencies, but the unit feature sizes are 10 pixels, 20 pixels and 8 pixels for the square wave, checkerboard and blue noise patterns, respectively. Visual inspection has confirmed that the different types of stimuli have roughly the same perceived contrast when their apparent radial frequencies are equal. There is another way to adjust the apparent frequency of the blue noise pattern by changing the dot distribution pattern. However, the possible range of the apparent frequencies by changing the dot pattern is very limited for a given level, for example, a 50% blue noise pattern. Therefore, we chose to use a fixed 50% blue noise pattern and changed the apparent frequency by adjusting the dot size.

According to the apparent frequency analysis, the unit feature sizes of the checkerboard gratings and blue noise patterns were designed so that their apparent frequencies matched those of the square wave gratings. Accordingly, the unit feature sizes of the checkerboard gratings

were chosen as: 40, 30 and 20 pixels for $\Delta L^* = 6.39$; 30, 20 and 15 pixels for $\Delta L^* = 12.7$; and 30, 20 and 12 pixels for $\Delta L^* = 25.5$, respectively. Likewise, the unit feature sizes of the blue noise patterns were: 15, 12 and 8 pixels for $\Delta L^* = 6.39$; 12, 8 and 6 pixels for $\Delta L^* = 12.7$; and 12, 8 and 5 pixels for $\Delta L^* = 25.5$, respectively. The unit feature sizes and their corresponding apparent frequencies are summarized in Table III.

Experimental Design and Procedure

A similar procedure to that described earlier for the square wave gratings was used to test these two types of stimuli. (The very low frequency 0.5 cpd gratings were not included in the new experiment.) The frequencies were adjusted by changing the unit feature sizes of the patterns. The frequency settings for the three types of gratings and the standard stimuli with different amplitudes are listed in Table IV.

For some of the frequencies, the experiments were conducted at various amplitudes and different types of patterns. For example, for frequencies 8 cpd and 12 cpd, the standard patches were modulated at all of the three amplitudes for checkerboard and blue noise patterns, and modulated at two amplitudes for the square wave grating. Thus the lightness difference perception can be analyzed based on the frequency, the modulation amplitude, and type of gratings.

The same five subjects in the square wave grating experiment participated in the two experiments using the checkerboard and blue noise patterns as the stimuli. As in the previous experiment, subject MW took part in the experiment twice, so in total six observations from five subjects were obtained.

Results

The average results for the checkerboard and blue noise patterns together with standard errors are plotted in Figs. 10 and 11, respectively.

Analysis

By inspecting the results, we can see that the frequency effect observed in Fig. 3 was repeated for the checkerboard gratings and blue noise patterns. The re-

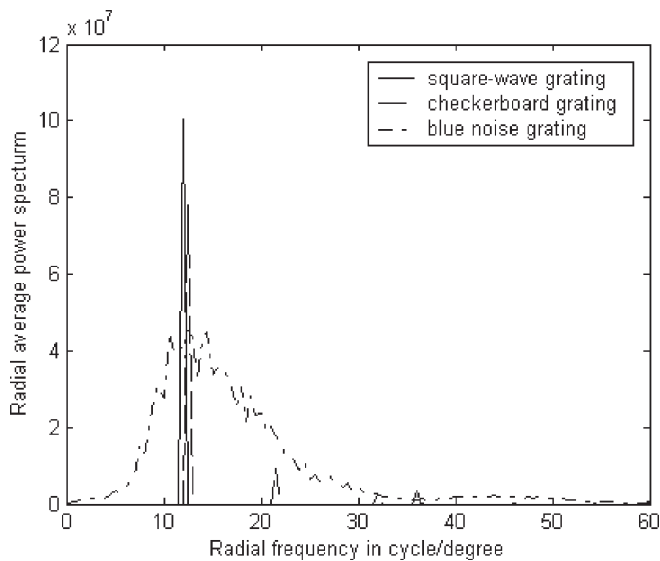


Figure 9. The radial average power spectrum of the square wave, checkerboard gratings and blue noise patterns, where the unit feature sizes of the square wave grating, the checkerboard grating and the blue noise pattern are 10 pixels, 20 pixels and 8 pixels, respectively. The three patterns have approximately the same dominant frequency. Solid line: square wave grating, dashed line: checkerboard grating, and dashed-dotted line: blue noise pattern. The amplitude of the RAPS of blue noise pattern is magnified by 15 to fit the scale.

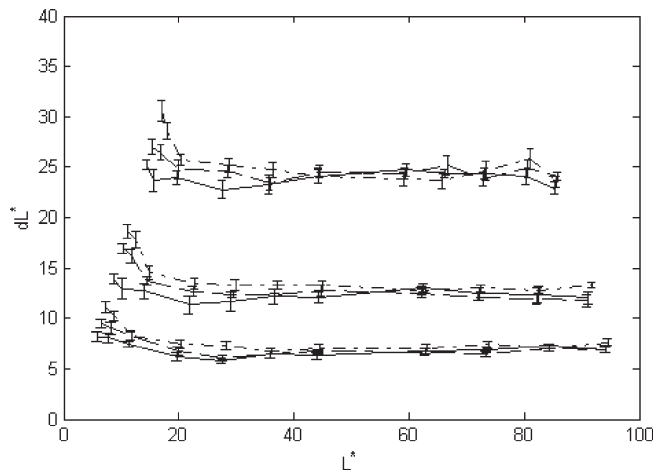


Figure 10. The average results of the six observations for the checkerboard patterns. The meanings of the x, y axes and the curves are the same as Fig. 3. For the groups of curves from the bottom to the top, the amplitudes were: $\Delta L^* = 6.39$, $\Delta L^* = 12.7$, and $\Delta L^* = 25.5$, respectively. For the group of curves on the bottom: solid line: 6 cpd, dashed line: 8 cpd, and dotted line: 12 cpd; for the group of curves in the center: solid line: 8 cpd, dashed line: 12 cpd, and dotted line: 15 cpd; for the group of curves on the top: solid line: 5 cpd, dashed line: 12 cpd, and dotted line: 20 cpd.

TABLE III. The Unit Feature Sizes in Pixel for the Square wave, Checkerboard and Blue Noise Patterns and the Corresponding Apparent Frequencies in Cycle/Degree.

Frequency	6 cpd	8 cpd	12 cpd	15 cpd	20 cpd
Square wave	20	15	10	8	6
Checkerboard	40	30	20	15	12
Blue noise	15	12	8	6	5

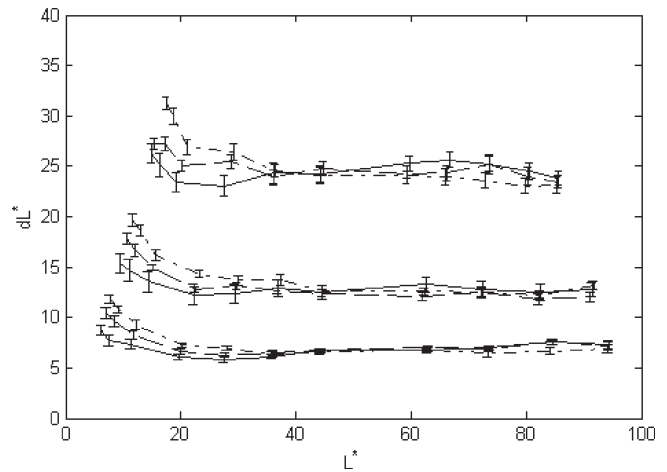


Figure 11. The average results of the six observations for the blue noise patterns. The meanings of the x, y axes and the curves are the same as Fig. 3. For the groups of curves from the bottom to the top, the amplitudes were: $\Delta L^* = 6.39$, $\Delta L^* = 12.7$, and $\Delta L^* = 25.5$, respectively. For the group of curves on the bottom: solid line: 6 cpd, dashed line: 8 cpd, and dotted line: 12 cpd; for the group of curves in the center: solid line: 8 cpd, dashed line: 12 cpd, and dotted line: 15 cpd; for the group of curves on the top: solid line: 8 cpd, dashed line: 12 cpd, and dotted line: 20 cpd.

TABLE IV. The Selection of the Dominant Frequencies for the Three Types of Stimuli Modulated at Different Amplitudes. The Cell With An “x” Mark Indicates that this Setting (The Grating Type, Amplitude and Frequency) Was Examined in the Experiment. SW: Square wave Grating, CB: Checkerboard Grating, and BN: Blue Noise Grating.

	$\Delta L^* = 6.39$			$\Delta L^* = 12.7$			$\Delta L^* = 25.5$		
	SW	CB	BN	SW	CB	BN	SW	CB	BN
0.5 cpd	x			x			x		
6 cpd		x	x						
8 cpd	x	x	x	x	x	x		x	x
12 cpd	x	x	x		x	x	x	x	x
15 cpd				x	x	x			
20 cpd							x	x	x

sults from the two tailed student *t*-test similar to Table II supported our observation that the frequency effect is significant at low L^* values but not at middle and high L^* values. The matching curves bend up for low L^* values and tend to be flat for middle L^* and high L^* values in Fig. 10 and Fig. 11. The higher the frequency, the more the curves bend for low L^* values, and the curves are displaced in the order of their frequencies.

Similar analyses as that described for square wave gratings in the last section were done for the checkerboard and blue noise patterns. First, using Eq. 5, the approximations of the first order differentiation of L_e^* versus L^* were obtained. Then these derivatives were fitted using the formula expressed by Eq. 6. Figure 12 illustrates the derivatives estimated from the experimental data for the checkerboard patterns (the isolated points) and the corresponding fitted curves with $\Delta L^* = 6.39$, $\Delta L^* = 12.7$ and $\Delta L^* = 25.5$, respectively. Finally, numerical integration was applied to the curves plotted in Fig. 12 and the mappings from the conven-

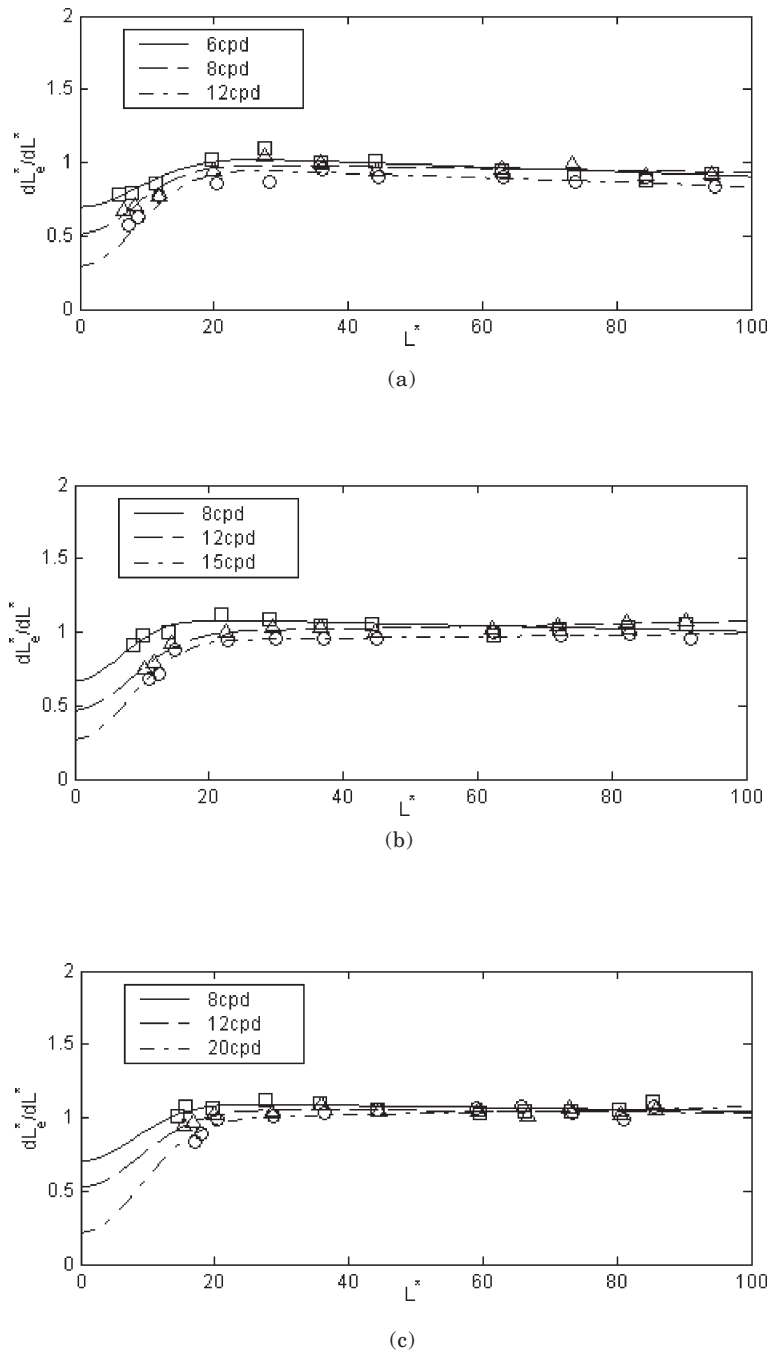


Figure 12. dL_e^*/dL^* . (a) $\Delta L^* = 6.39$, (b) $\Delta L^* = 12.7$, and (c) $\Delta L^* = 25.5$. Checkerboard grating.

tional L^* to the effective L_e^* at various frequencies and amplitudes were established, as illustrated in Fig. 13.

Likewise, the first order derivatives and the fitted curves for blue noise patterns are illustrated in Fig. 14, and the mapping curves from L^* to L_e^* are illustrated in Fig. 15 for different frequencies and amplitudes.

As with the square wave gratings, the frequency effect for spatially modulated checkerboard and blue-noise patterns is clearly observable in these figures, and the amplitude effect is not significant compared

to the frequency effect. Another interesting issue is whether there is an effect related to the type of the modulation. The two L_e^* curve shown in Fig. 16 are the average L_e^* ($f = 8$ cpd) of checkerboard pattern and blue noise pattern and the average L_e^* ($f = 12$ cpd) of checkerboard pattern and blue noise pattern, plotted by solid line and dashed line, respectively. The error bars on the curves are the deviation of each individual L_e^* curve from the average L_e^* curve at the given frequency. Figure 16 suggests that the magnitude of the

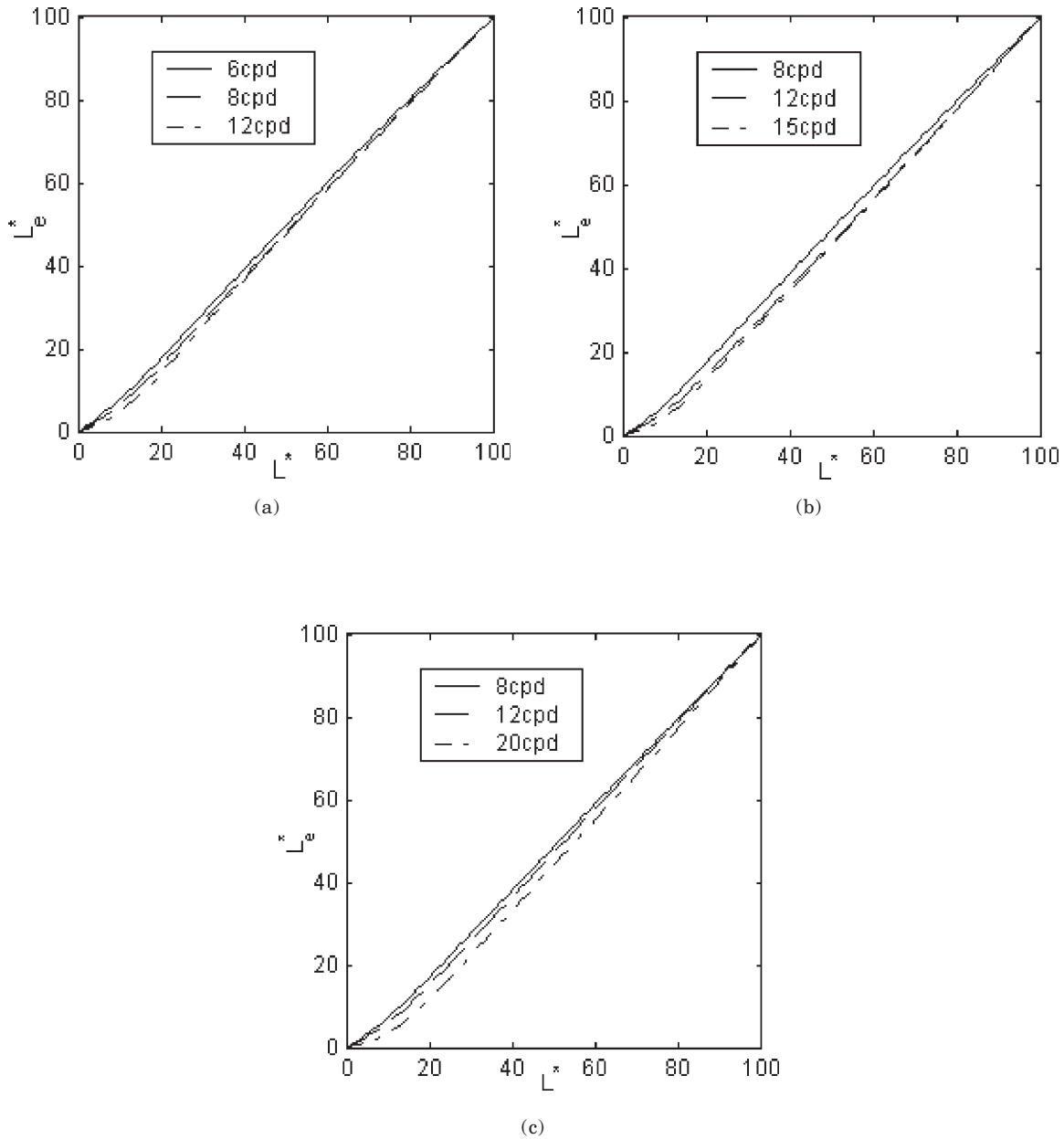


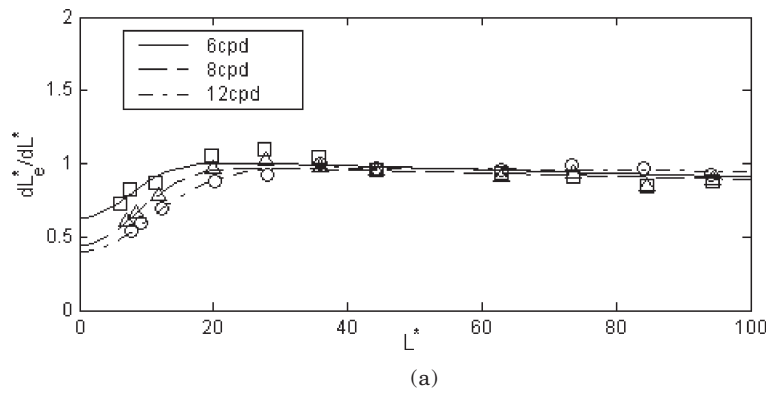
Figure 13. L_e^* versus L^* . (a) $\Delta L^* = 6.39$, (b) $\Delta L^* = 12.7$, and (c) $\Delta L^* = 25.5$. Checkerboard grating.

modulation type effect is smaller than that of the frequency effect.

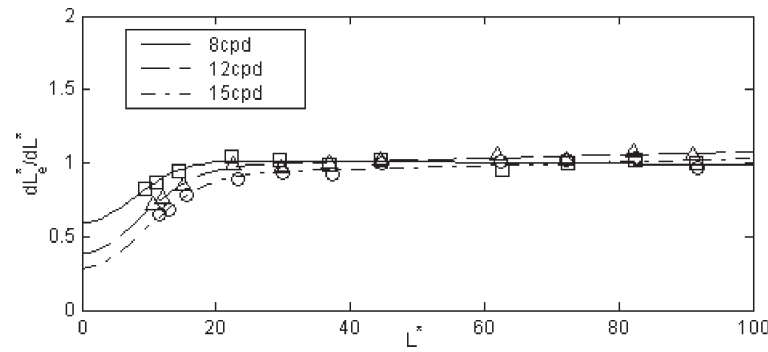
Furthermore, the differences among the L_e^* values for various amplitudes and modulation types do not exhibit an ordered pattern as those caused by frequency variation. Therefore, we infer that the frequency effect dominates the lightness difference perception for spatially modulated signals and the effect of amplitude and modulation type may be ignored in our analyses. Thus, the L_e^* can be expressed as a function of the apparent frequency

only, regardless of the modulation amplitude and modulation type. The family of curves from 6 cpd to 20 cpd for checkerboard gratings and blue noise patterns are illustrated in Fig. 17 with frequency as the parameter. Each curve is the average of the curves with the same frequency but different amplitudes.

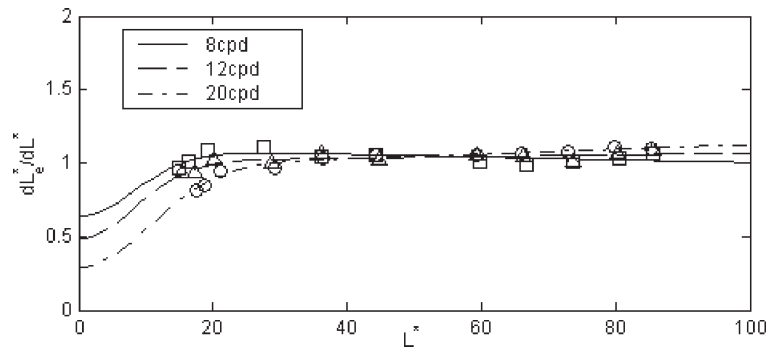
In a multi-level printing system, the modulation frequency in the experiment is related to the printing resolution, the modulation amplitude is related to the number of output levels, and the modulation type is re-



(a)



(b)



(c)

Figure 14. dL_e^*/dL^* . (a) $\Delta L^* = 6.39$, (b) $\Delta L^* = 12.7$, and (c) $\Delta L^* = 25.5$. Blue noise grating.

lated to the multitone scheme. Therefore, in order to determine the optimal intermediate output levels, for a certain type of halftone scheme, the printing resolution and the assumed typical viewing distance will be enough to develop the optimal L_e^* curve, no matter how many output levels are used.

Parameterize the Frequency

From the experimental results, the L_e^* versus L^* function can be determined for the frequencies that were

studied in the experiment. In order to easily apply these results to multitone applications, it is desirable to generalize the $L_e^*(f)$ function so that an effective lightness space can be obtained for an arbitrary apparent frequency. For the reason of simplicity and clarity, the analyses are based on the results of blue noise patterns throughout the subsequent part of this study.

It was observed that the dL_e^*/dL^* curves exhibit a certain pattern according to their apparent frequency. Let us consider the derivatives of the difference between L^*

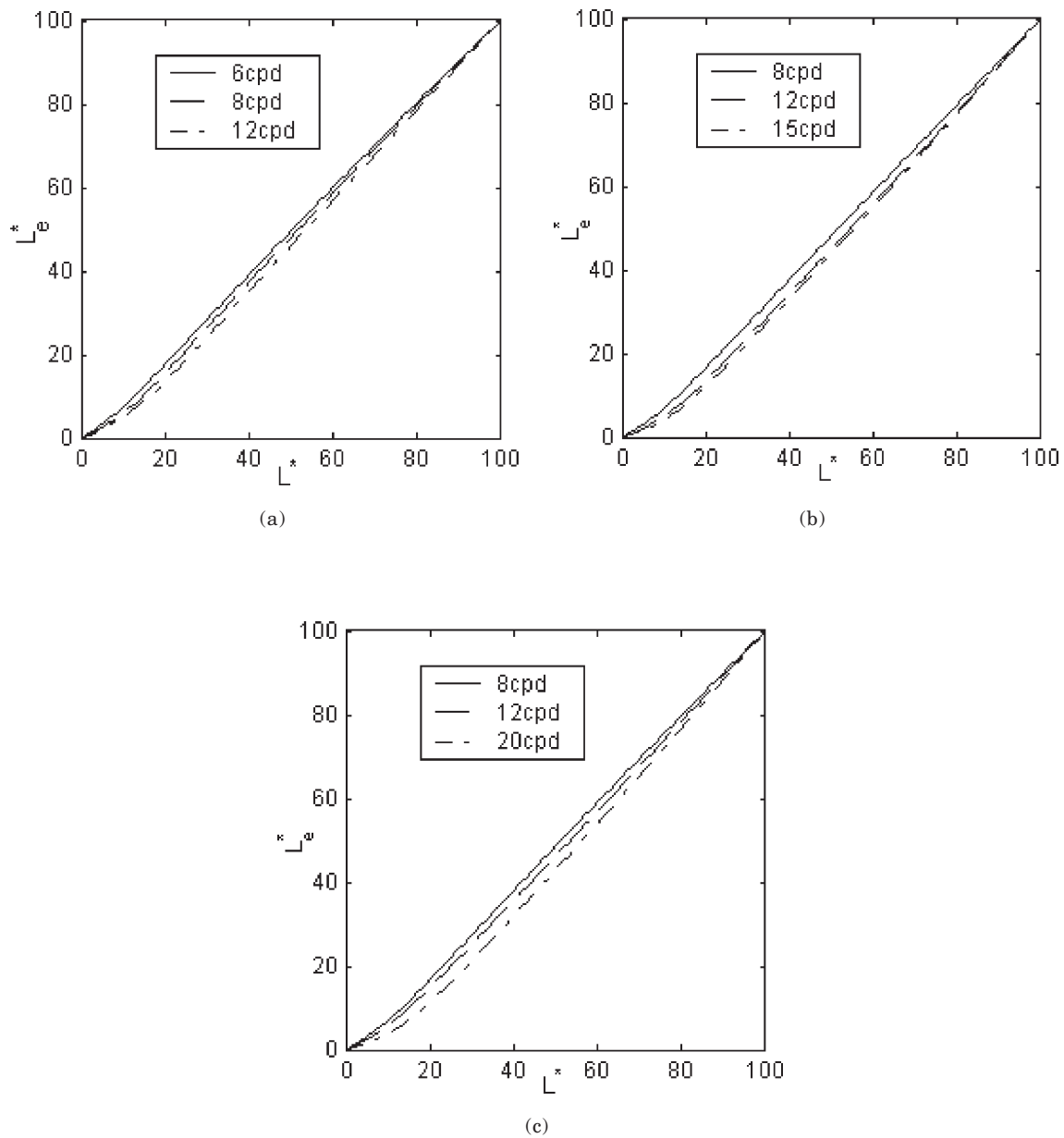


Figure 15. L_e^* versus L^* . (a) $\Delta L^* = 6.39$, (b) $\Delta L^* = 12.7$, and (c) $\Delta L^* = 25.5$. Blue noise pattern.

and L_e^* as a function of L^* , $d(L^*-L_e^*)/dL^*$, which is equal to $1-dL_e^*/dL^*$. According to Eq. 6, the $d(L^*-L_e^*)/dL^*$ function can be expressed by:

$$\frac{d(L^* - L_e^*)}{dL^*} = 1 - \frac{dL_e^*}{dL^*} = 1 - (a_1 + a_2 L^*) \left(1 - a_3 \exp(-a_4 L^{*2}) \right) \quad (9)$$

Figure 18 illustrates a family of $d(L^*-L_e^*)/dL^*$ curves for different frequencies for the blue noise patterns, corresponding to the dL_e^*/dL^* data given in Fig. 17(b). It can be easily observed that the curves arrange in a regular progression. It is reasonable to assume that the curve for a frequency between two experimental frequencies will be between the curves for these two frequencies. Likewise, the curve can be extrapolated for the frequencies that exceed the experimental frequencies if the extrapolated frequencies are within a certain limit. In

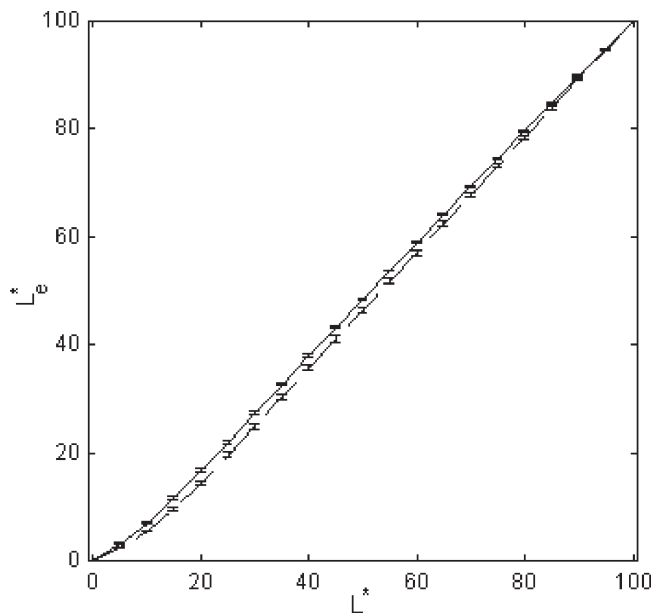
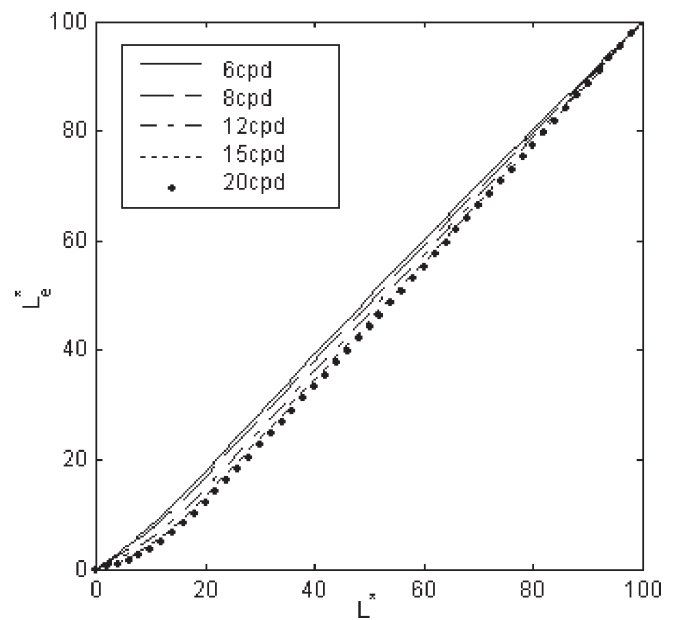


Figure 16. Average L_e^* (checkerboard and blue noise pattern) and the deviation from the average L_e^* versus L^* under frequencies 8 cpd (solid line) and 12 cpd (dashed line).

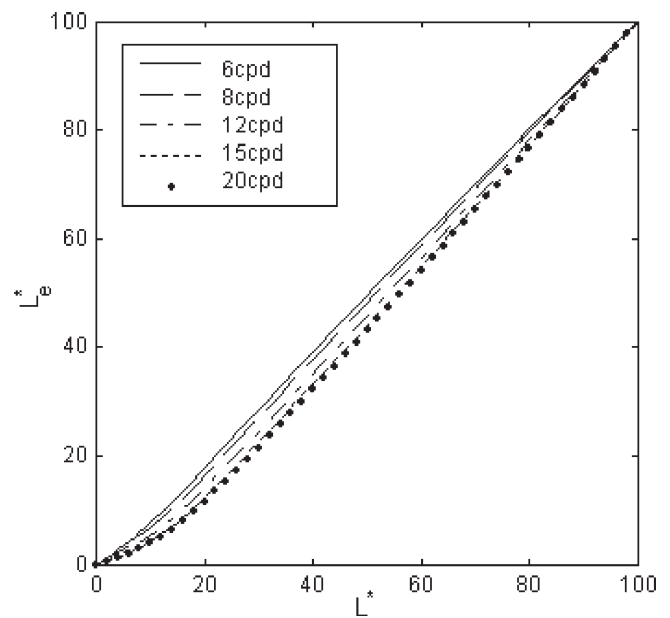
order to generalize the curves for arbitrary frequencies, a series of control points are determined for these curves that can be parameterized as a function of frequency. Since four parameters, a_1 , a_2 , a_3 and a_4 , are used to represent the function given in Eq. (9), at least four control points are required to reconstruct the curve. The four points that were chosen as the control points are illustrated in Fig. 18. The first point is on the left end of the curve ($L^* = 0$), which is represented by a diamond symbol, the second point is the point where $d(L^*-L_e^*)/dL^* = 0$, which is represented by an open circle symbol, the third point is the intersection point of all the curves, which is represented by a star symbol, and the fourth point is on the right end of the curve ($L^* = 100$), which is represented by a triangle symbol. The first and the fourth points are at the lowest and highest values of L^* . The second point is where the L_e^* has the largest deviation from L^* . The selection of the third control point is primarily according to visual inspection, and it is determined empirically. It is further assumed that the curves $d(L^*-L_e^*)/dL^*$ for other frequencies will pass through the third control point, and that the locations for each of the other three points will conform to a linear relationship with respect to the frequency, which can be derived by linear regression from the experimental data shown in Fig. 18.

After the four points are determined, the four parameters in Eq. (9) can be determined using the method of minimizing mean square error. Thus, the dL_e^*/dL^* for frequencies between the experimental values or beyond the experimental values can be evaluated by interpolation or extrapolation.

The procedure to generate an L_e^* function at any given frequency is as follows: first, four control points on the $d(L^*-L_e^*)/dL^*$ curve are found; second, the four parameters a_1 , a_2 , a_3 , and a_4 in Eq. (9) are calculated using least mean square error algorithm, and then we obtained the formula of dL_e^*/dL^* ; third, L_e^* is acquired by numerical inte-



(a)



(b)

Figure 17. The average mapping curves from L^* to L_e^* as a series of apparent frequency values. (a): Checkerboard gratings, and (b): Blue noise patterns.

gration. The equations used to determine the coordinates of the four points are listed in Table V. For example, if we want to find the $L_e^*(f = 16 \text{ cpd})$, we first determine the coordinates of the four control points on the $d(L^*-L_e^*)/dL^*$ curve, and solve the four parameters in Eq. (6), and then $L_e^*(f = 16 \text{ cpd})$ can be obtained by taking the numerical integration of the dL_e^*/dL^* function. This L_e^* function is suitable for different amplitudes and different modulation patterns. The values of the four control points and four parameters for $f = 16 \text{ cpd}$ and $f = 24 \text{ cpd}$ and

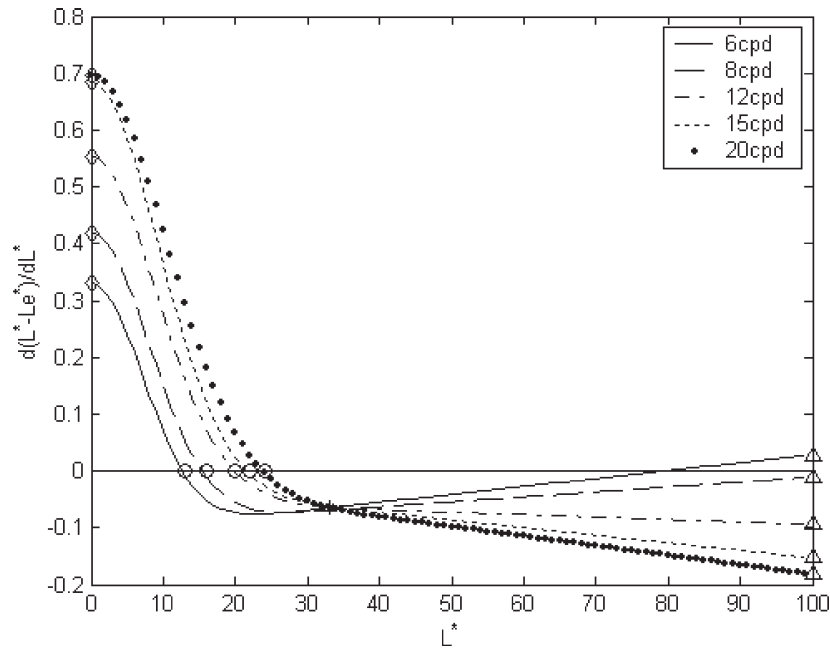


Figure 18. $d(L^*-L_e^*)/dL^*$ as a function of frequency (blue noise pattern). In this figure, for each curve, four points are selected: $d(L^*-L_e^*)/dL^*$ ($L^* = 0$) (represented by diamond symbols), $d(L^*-L_e^*)/dL^*$ ($L^* = 100$) (represented by triangle symbols), $d(L^*-L_e^*)/dL^* = 0$ (represented by open circle symbols), and the point where the five curves intersect (represented by a star symbol).

TABLE V. The Coordinates of the Four Control Points. In the Figure, f is the Apparent Frequency in the Unit of Cycle/Degree.

	Point 1	Point 2	Point 3	Point 4
Coordinate in (L^* , $d(L^*-L_e^*)/dL^*$) plot	(0, $0.2+0.0276*f$)	($9.52+0.777*f$, 0)	(33, -0.065)	(100, $0.107-0.0155*f$)

TABLE VI. The Coordinates of the Four Control Points for Various Frequencies.

	Point 1	Point 2	Point 3	Point 4
coordinate in (L^* , $d(L^*-L_e^*)/dL^*$) plot				
10 cpd	(0, 0.4763)	(17.29, 0)	(33, -0.065)	(100, -0.048)
15 cpd	(0, 0.6143)	(21.18, 0)	(33, -0.065)	(100, -0.126)
16 cpd	(0, 0.6419)	(21.95, 0)	(33, -0.065)	(100, -0.141)
20 cpd	(0, 0.7523)	(25.06, 0)	(33, -0.065)	(100, -0.203)
24 cpd	(0, 0.8627)	(28.17, 0)	(33, -0.065)	(100, -0.265)
25 cpd	(0, 0.8903)	(28.95, 0)	(33, -0.065)	(100, -0.281)
27.5 cpd	(0, 0.9593)	(30.89, 0)	(33, -0.065)	(100, -0.319)

TABLE VII. The Parameters Used To Fit The Eq. 9 For Various Frequencies.

	a_1	a_2	a_3	a_4
10 cpd	1.0738	-2.580×10^{-4}	0.5123	6.914×10^{-3}
15 cpd	1.0377	8.780×10^{-4}	0.6283	5.502×10^{-3}
16 cpd	1.0310	1.110×10^{-4}	0.6527	5.238×10^{-3}
20 cpd	1.0100	1.930×10^{-4}	0.7547	4.166×10^{-3}
24 cpd	1.0256	2.393×10^{-4}	0.8661	2.923×10^{-3}
25 cpd	1.0540	2.265×10^{-4}	0.8959	2.538×10^{-3}
27.5 cpd	1.5358	-2.165×10^{-4}	0.9735	1.169×10^{-3}

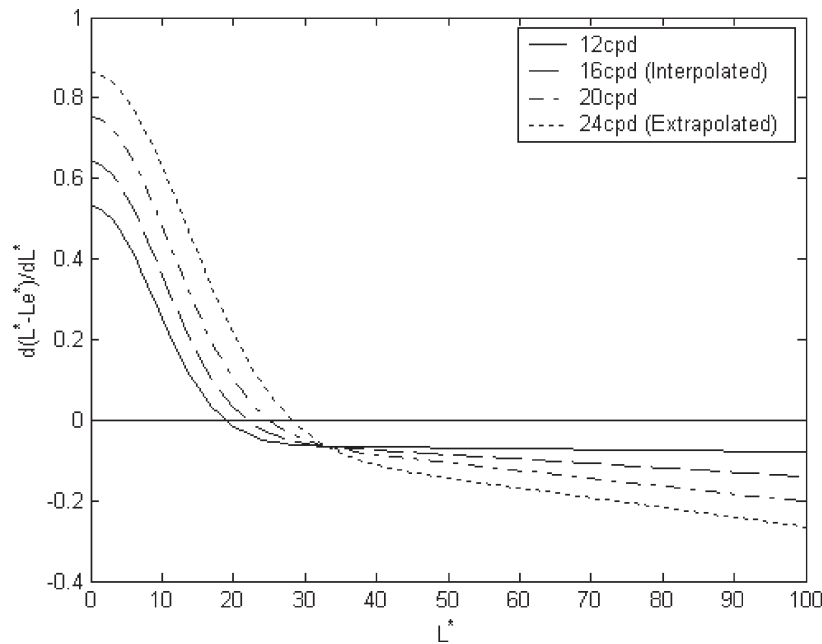


Figure 19. The predicted $d(L^*-L_e^*)/dL^*$ as a function of frequency. Blue noise pattern. The 16 cpd is obtained by interpolation, and the 24 cpd is obtained by extrapolation.

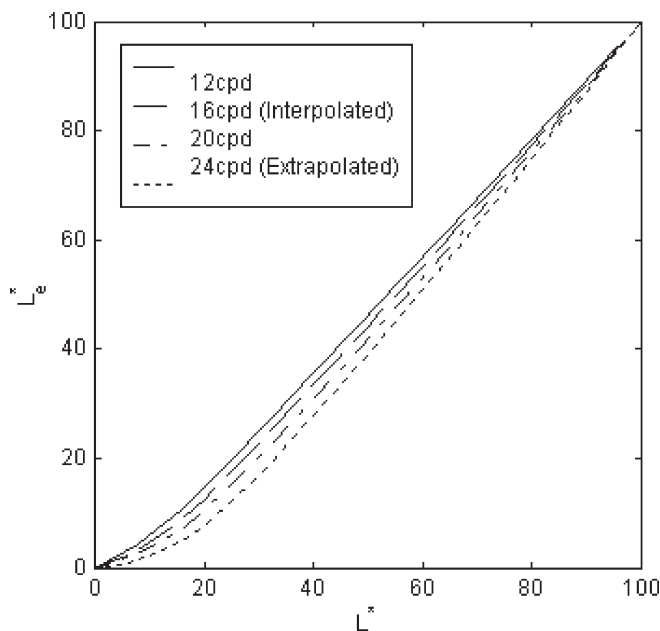


Figure 20. The resulting L_e^* versus L^* mapping function.

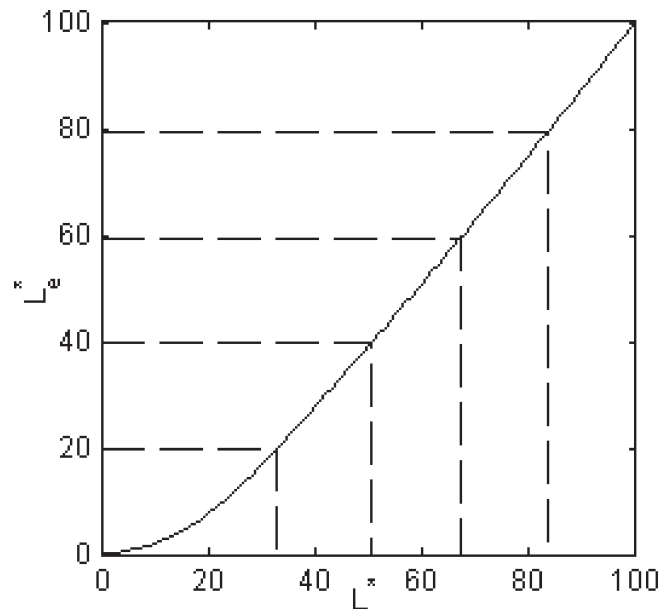


Figure 21. The scheme to select the intermediate output levels for multitone, such that the levels are equally spaced in L_e^* .

other frequencies are listed in Table VI and Table VII, respectively. The illustration of the resulting $d(L^*-L_e^*)/dL^*$ curves for $f = 16, 24$ and L_e^* for $f = 16, 24$ are plotted in Fig. 19 and Fig. 20, respectively.

The Application of L_e^* to the Selection of Optimal Output Levels for Multitone

Perceived Lightness Difference in the L_e^* Space

The L_e^* space is derived based on the experimental results of the perception of modulated stimuli. Accord-

ing to the motivation of designing this experimental study, levels that are equally spaced in L_e^* should produce equal lightness difference perception for halftone patterns with the corresponding apparent frequency. Figure 21 illustrates a method for selecting the optimal output levels for multitone using L_e^* to produce uniform visibility across the tone scale for a frequency of interest. First, select L_e^* values that are equally spaced in the L_e^* space, then the corresponding L^* values are determined using the relationship between L_e^* and L^* . The lightness values represented by L^* are the selected

TABLE VIII. The L^* Values of the Six Levels That Are Equally Spaced In The Effective Lightness Space L_e^* And The Conventional L^* . Note That The Lowest L^* Value That Can Be Reproduced On The Paper Is 5.41, Calculated Using the Calibration Table.

	L_1^*	L_2^*	L_3^*	L_4^*	L_5^*	L_6^*
Conventional L^*	5.41	24.32	43.25	62.16	81.08	100
L_e^* ($f = 20$ cpd)	5.41	30.47	48.65	66.24	83.34	100
L_e^* ($f = 25$ cpd)	5.41	33.77	51.32	68.06	84.27	100
L_e^* ($f = 27.5$ cpd)	5.41	37.11	53.51	69.10	84.57	100

output levels for multitoning.

Experiment to Verify Lightness Difference Uniformity of L_e^* Space

A visual experiment was conducted to verify whether L_e^* can produce uniform lightness difference perception for spatially modulated patterns. The stimuli were 50% monochromatic gray blue noise patterns modulated at levels that are equally spaced in L_e^* for several frequencies. The frequencies for L_e^* were chosen as 20 cpd, 25 cpd, and 27.5 cpd, together with the conventional L^* . For each dominant frequency, six gray levels were selected that were uniformly spaced in effective lightness, and five 50% halftone patterns modulated by every two adjacent levels were generated. The corresponding L^* values used in this experiment are listed in Table VIII.

Each stimulus was a 5 in. \times 5 in. (13 cm \times 13 cm) square. The resolution of the prints was 50 dpi, and the prints were presented to the subjects at the distance of 4.5 ft. (1.36 m). Under this condition, the apparent frequency of the prints is 20 cpd. The illuminant is white light with color temperature of 5000K. The observers viewed the stimuli binocularly.

For each test stimulus, the subject was asked to choose one of the standard gratings whose visibility was closest to that of the experimental patch. The set of the standard gratings comprised ten 50% blue noise patches that had contrasts varying in approximately equal steps from 1 to 10 (arbitrary units), with a smaller number indicating lower contrast and a larger number indicating higher contrast. The contrast scale is measured by the lightness difference between the modulated levels. The average lightness values for the standard patterns were about 60, in which the L_e^* is approximately linearly related to L^* . Considering that the frequency dependent effect is only found at low lightness intensities, the contrasts of the standard gratings should be equally stepped as well. All the test stimuli and standard gratings have the same halftone noise patterns, and they are only different in the modulation levels.

The average result of the six observers is plotted in Fig. 22 and listed in Table IX, respectively. The relative visibility of each pattern is the average value of the visibility represented by the visibility scale of the standard gratings from 1 to 10. The second to the right column

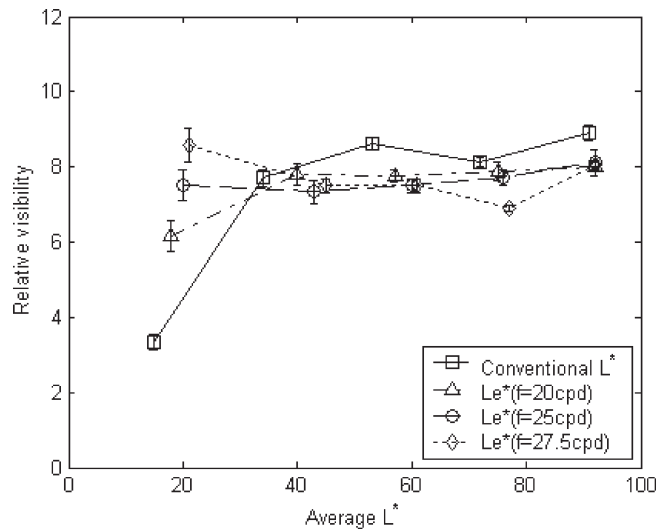


Figure 22. The relative visibility of the halftone patterns.

is the standard deviation of the relative visibility varying with the lightness value, and the rightmost column is the difference between the maximal and minimal relative visibility. It can be seen that levels equally spaced in the conventional L^* space do not lead to equal contrast perception. There is a significant drop of the perceived difference at low L^* . As expected, uniformly spacing the levels in effective lightness produces more uniform visibility at different intensities relative to uniformly spacing the levels in L^* . More specifically, L_e^* ($f = 25$ cpd) provides the most consistent contrast perception across the tonal range, whereas L_e^* ($f = 20$ cpd) under corrected the deficiency of L^* , and L_e^* ($f = 27.5$ cpd) over corrected the deficiency of L^* .

It is also interesting to point out that, although under this viewing distance, the blue noise pattern had the apparent frequency of 20 cpd, L_e^* ($f = 20$ cpd) did not produce the most uniform visibility. In this case, L_e^* ($f = 25$ cpd) provides the best results. The possible reason for this could be that the viewing conditions for the prints were somewhat different than that of the CRT display used in the earlier experiments with respect to surround, etc, so there may be some adaptation effect that has not been accounted for. In a practical multitoning application, the appropriate apparent frequency that should be used to compute the optimal L_e^* curve must be determined empirically.

Multilevel Halftoning Simulation Using L^* and L_e^*

We also generated the 4-level halftone prints of grayscale ramps and real images using L^* , L_e^* ($f = 20$ cpd) and L_e^* ($f = 25$ cpd). The texture visibility of the ramps using L_e^* ($f = 20$ and 25 cpd) is more uniform than that produced using L^* . The texture looks much smoother using L_e^* than using L^* in large areas with gradually changed intensities.†

TABLE IX. The Relative Visibility of the Halftone Patterns.

Pattern	(L_1^*, L_2^*)	(L_2^*, L_3^*)	(L_3^*, L_4^*)	(L_4^*, L_5^*)	(L_5^*, L_6^*)	STD	Max - Min
Conventional L^*	3.33	7.71	8.63	8.13	8.92	2.29	5.58
L_e^* ($f = 20$ cpd)	6.17	7.79	7.75	7.88	8.00	0.76	1.83
L_e^* ($f = 25$ cpd)	7.50	7.33	7.50	7.71	8.13	0.31	0.79
L_e^* ($f = 27.5$ cpd)	8.58	7.50	7.50	6.92	8.04	0.63	1.67

Conclusions

In this study, psychophysical experiments were described investigating lightness difference perception for spatially modulated patterns using a lightness difference matching paradigm. Various types of patterns were used to study the effect of modulation frequency and modulation amplitude on the perception of lightness differences for square wave, checkerboard, and blue noise patterns. The perception for a particular modulation frequency, amplitude, and modulation type is analogous to the perception of multitone patterns generated by the corresponding printing resolution, number of output levels, and type of halftone scheme.

Based on the experimental results, an effective lightness scale L_e^* is obtained for each frequency, amplitude and modulation type. The results show that effective lightness difference perception is reduced at low L^* values under high frequencies, and the magnitude of this frequency effect is highly related to the modulated frequency. It is also shown that the modulation amplitude and modulation type do not induce an observable effect on lightness difference perception compared to the frequency effect. Thus, the L_e^* function is dependent only on the apparent spatial frequency, regardless the modulation amplitude and modulation type. Furthermore, the corresponding L_e^* function can be determined for a given frequency by numerical estimation. Further visual experiments and simulated prints showed that equally spacing multitone levels in L_e^*

produced halftone patterns where the pattern visibility is significantly more uniform than when the levels are equally spaced in L^* . 

References

1. R. Miller and C. Smith, Mean-preserving multilevel halftoning algorithm, *Proc. SPIE*, **1913**, 367-377 (1993).
2. Q. Yu, K. J. Parker, K. Spaulding, and R. Miller, Improved digital multitone with over-modulation scheme, *Proc. SPIE*, **3300**, 362-373 (1998).
3. CIE, *Colorimetry*, 2nd Ed., Publication CIE, No. 15.2, 1986, Section 4, Recommendations concerning uniform color spacing.
4. Q. Yu, K. J. Parker, K. Spaulding, and R. Miller, Digital multitone with overmodulation for smooth texture transition, *J. Electronic Imaging*, **8**(3), 311-321 (1999).
5. M. Wang, K. J. Parker, K. E. Spaulding, Q. Yu, and R. L. Miller, Perceived lightness difference with regard to spatial frequency and amplitude modulation, *Proc. SPIE*, **3959**, 16-27 (2000).
6. H. Pauli, Proposed extension of the CIE coordinated research on uniform color spaces, color difference equations, and metric color terms, *J. Opt. Soc. Amer.*, **66**, 866-867 (1976).
7. R. J. Snowden and S. T. Hammett, The effects of surround contrast on contrast thresholds, perceived contrast and contrast discrimination, *Vision Res.* **38**, 1935-1945 (1998).
8. Y. Ejima and S. Takahashi, Apparent contrast of a sinusoidal grating in the simultaneous presence of peripheral gratings, *Vision Res.* **25**, 1223-1232 (1985).
9. E. Peli, L. Arend and A. T. Labianca, Contrast perception across changes in luminance and spatial frequency, *J. Opt. Soc. Amer. A*, **13**(10), 1953-1959 (1996).
10. E. B. Goldstein, *Sensation and perception*, 4th Ed., Brooks/Cole Publishing Company, Pacific Grove, CA, 1996, Chap. 5, pp. 211-217.
11. R. A. Ulichney, Dithering with blue noise, *Proc. IEEE*, **76**, 56-79 (1988).

† All the images of multitone prints were simulated with a modified Kodak Approval printer that is designed and built as a color proofer for graphic arts application. With a maximum addressable printing resolution of 1800 dpi, this printer is well suited as an output device for generating simulated multilevel ink jet prints. However, due to difficulties accurately reproducing the L^* values in publication, these multilevel halftoned examples will not be included in this article.